ISSN 1070-3632, Russian Journal of General Chemistry, 2023, Vol. 93, No. 1, pp. 85–90. © Pleiades Publishing, Ltd., 2023.

Successive Ionic layers Deposition of Multilayers of $[n(Co(OH)_2–mPt(0)]_k$ Nanocomposites and Their Structural and Chemical Features

V. P. Tolstoy[a],* and M. V. Kaneva[a]

[a] *Institute of Chemistry, St. Petersburg State University, St. Petersburg, 198504 Russia*
**e-mail: v.tolstoy@spbu.ru*

Received November 10, 2022; revised November 23, 2022; accepted November 25, 2022

Abstract—Repeated and alternate treatment of a nickel surface with Na_2PtCl_6, $CoCl_2$, and $NaBH_4$ solutions with the general formula $[n(Co(OH)_2–mPt(0)]_k$ (*n* and *m* denote the number of Successive Ionic layers Deposition (SILD) cycles in the preparation of $Co(OH)_2$ and Pt(0), respectively, and *k* is the number of their repetitions] leads to the formation of multilayer nanocomposites consisting of $Co(OH)_2$ nanosheets and Pt(0) nanoparticles. Their studying by TEM, SEM, XPS, and X-ray diffraction methods showed that it is possible to change morphological characteristics of both nanosheets and nanoparticles, and also of the arrays which they form, by changing the synthesis program, i.e., for example, the *n* and *m* values. The most significant differences in such characteristics are observed for samples obtained at *n* and *m* values preset in the range of 1–5. The study of the electrocatalytic behavior of such samples in the reaction of hydrogen evolution during the electrolysis of water in the alkaline region showed that the overvoltage values in the series of such samples are largely determined by the synthesis conditions, and their analyzing in the series of samples obtained according to various algorithms allows us to choose the conditions that provide the lowest overvoltage values.

Keywords: multilayers, Pt(0) nanoparticles, $Co(OH)_2$ nanosheets, composites, SILD, hydrogen evolution reaction, electrolysis of water

DOI: 10.1134/S1070363223010127

As is known, new possibilities in obtaining multilayers of inorganic and inorganic-organic compounds on the surface of various substrates are opened up by methods of their layer-by-layer precision synthesis. Among such methods there is the method of Atomic Layer Deposition (ALD), which allowed earlier, for example, the so-called laminar multilayers of the "superlattice" type to be obtained [1–4]. At the same time, the first experiments on the synthesis of such multilayers by the Successive Ionic Layers Deposition (SILD) showed that, when obtaining a number of metal oxides and hydroxides, for example, layered double hydroxides ZnCoOH [5], CoAlOH [6], and ZnFeOH [7], layers formed on the surface present a set of ultra-thin nanosheets of a nanometer thickness with a distorted planar geometry. As a consequence, this leads to significant problems in the formation of such laminar multilayers. However, these results opened up the possibility of creating other important nanomaterials by the SILD method, namely, thin-layer structures consisting of unique arrays of oriented nanosheets with a highly developed surface. The study of their properties has shown that the noted features are extremely in demand when creating, for example, new electrodes for electrochemical energy storage devices or new electrocatalysts for various electrochemical processes, since it is precisely such nanostructures that contain a large number of adsorption centers, including catalytically active centers. Among electrocatalysts, Pt and Co nanocomposites and alloys exhibit unique electrocatalytic properties, in particular, in the reactions of methyl alcohol oxidation [8], Hydrogen Evolution Reaction (HER) during water electrolysis in the alkaline region [9–12], or oxygen reduction reactions [13–16]. This fact largely determined the particular range of samples under study. An analysis of the results presented in these works showed that these nanomaterials were obtained using solutions of platinum and cobalt salts and reducing agents as reagents in the so-called "mixed mode" rather than under conditions of "layer-by-layer" synthesis.

The aim of this work was to study the structural and chemical features of a series of multilayer nanocomposites

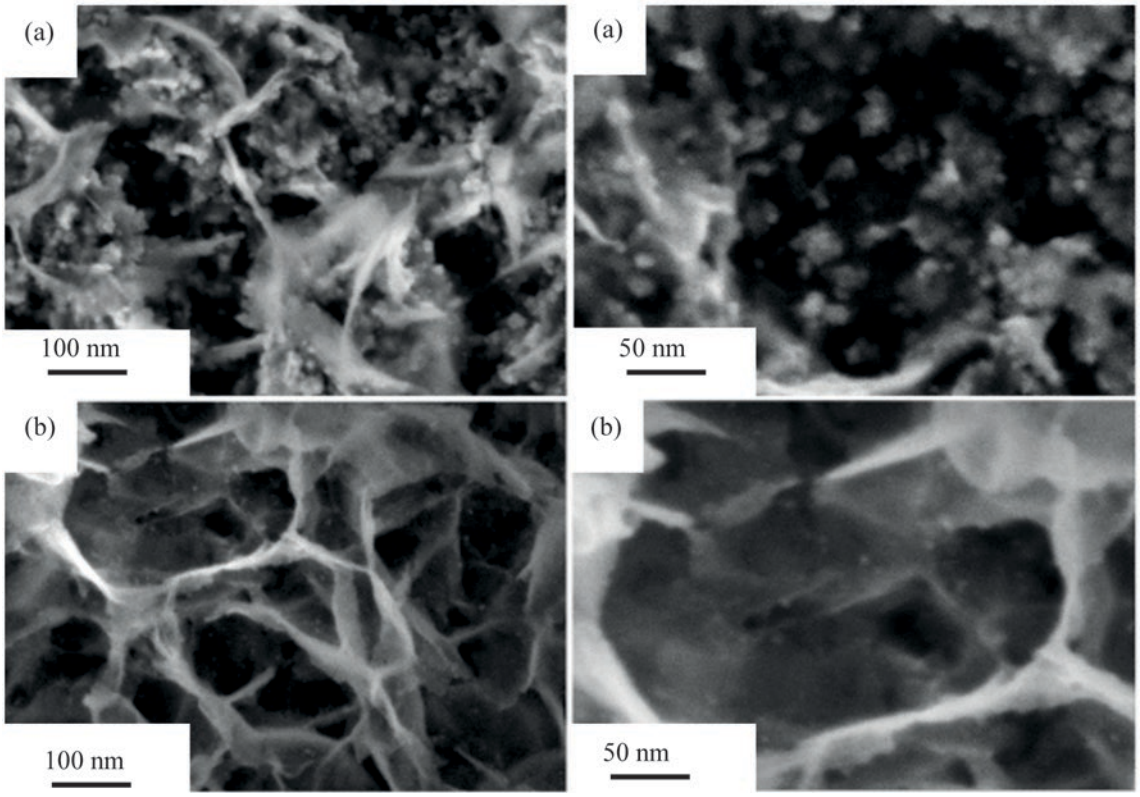

Fig. 1. SEM electron micrographs taken at various magnifications for (a) $[1Co(OH)_2–1Pt(0)]_{10}$ and (b) $[5Co(OH)_2–5Pt(0)]_2$ multilayers synthesized by the SILD method on a nickel surface.

containing such components as $Co(OH)_2$ nanosheets and Pt(0) nanoparticles synthesized by the SILD method.

Nickel foam plates and nickel foils, which are typical electrode bases in studies of electrochemical processes in alkaline media, were used as substrates in the synthesis. Multilayers of nanocomposites characterized by the general formula $[mCo(OH)_2–nPt(0)]_k$, which contains information about the synthesis program, were deposited on these substrates by the SILD method. According to this formula, when one of these samples was synthesized, for example, using the $[1Co(OH)_2–1Pt(0)]_{10}$ algorithm, this means that it was obtained as a result of one cycle of treating the substrate with $CoCl_2$ and $NaBH_4$ solutions and then one cycle with Na_2PtCl_6 and $NaBH_4$ solutions, and this sequence of treatments was repeated ten times.

The study of the synthesized samples by the SEM method showed that the morphology of the multilayers is largely determined by the synthesis algorithm (Fig. 1). For example, if a multilayer is synthesized using the $[1Co(OH)_2–1Pt(0)]_{10}$ program, then it consists of nanosheets with lateral sizes at the level of 100–150 nm and nanoparticles with sizes of about 5–20 nm, whereas if the algorithm is $[5Co(OH)_2–5Pt(0)]_2$, then it consists of nanosheets with similar sizes at the level of 200 and more nanometers and nanoparticles with sizes of about 5 nm.

Taking into account the results of works [17] and [18], in which the features of the SILD synthesis of nanolayers with reagent solutions of $CoCl_2$, $NaBH_4$ and H_2PtCl_6, $NaBH_4$, respectively, were studied, it can be assumed that $Co(OH)_2$ nanocrystals have the nanosheet morphology and Pt(0) – the nanoparticle morphology. An analysis of the microphotographs also allows us to conclude that the nanosheets are mainly oriented vertically with respect to the substrate surface and form peculiar arrays with open pores of sizes about 100 nm for the $[1Co(OH)_2–1Pt(0)]_{10}$ sample and 50–300 nm for the $[5Co(OH)_2–5Pt(0)]_2$ sample. As is known [19–21], it is precisely this orientation that sets relatively low values of overpotentials in many electrocatalytic reactions, including the water decomposition during

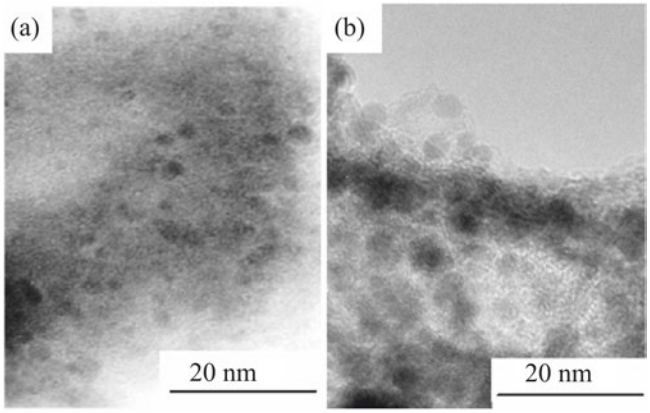

Fig. 2. TEM micrographs of fragments of (a) $[1Co(OH)_2–1Pt(0)]_{10}$ and (b) $[5Co(OH)_2–5Pt(0)]_2$ multilayers synthesized by the SILD method on a nickel surface.

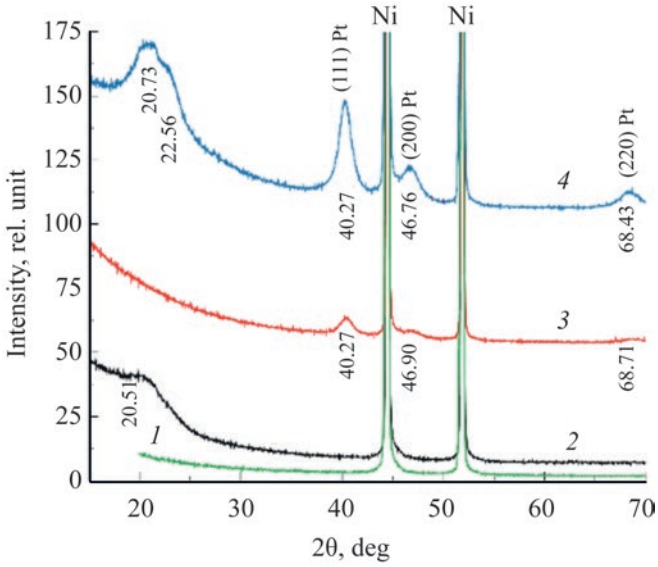

Fig. 3. X-ray diffraction patterns of nickel (*1*) and multilayers synthesized by the SILD method on its surface in accordance with (*2*) $[20Co(OH)_2]_1$, (*3*) $[1Co(OH)_2–1Pt(0)]_{20}$, and (*4*) $[5Co(OH)_2–5Pt(0)]_4$ programs.

its electrolysis, since the concentration of the dissolved gas in the gaps between the nanosheets turns out to be significantly higher than in the volume of the solution, and this contributes to the formation of gas bubbles in these areas at a lower overpotential on the electrode and to their subsequent separation from the electrode in the areas at the nanosheets tops.

In addition to the before-mentioned samples, $[10Co(OH)_2–10Pt(0)]_2$ and $[20Co(OH)_2–20Pt(0)]_2$ samples were studied by the SEM method. The analysis of micrographs of these samples showed that in these cases, nanocomposite layers consisting of a combination of nanosheets and nanoparticles are also formed on the surface, and their sizes turned out to be comparable with similar sizes of the samples synthesized in [17] and [18] devoted, as noted above, to the synthesis of $Co(OH)_2$ nanosheets and Pt(0) nanoparticles, respectively, and therefore these micrographs are not shown in Fig. 1.

Important information about the structural and chemical features of the above-noted samples was obtained as a result of their study by the TEM method (Fig. 2). It follows from the micrographs shown in this figure that the $[1Co(OH)_2–1Pt(0)]_{10}$ sample is formed by a combination of platinum nanoparticles 2–3 nm in size, and $[5Co(OH)_2–5Pt(0)]_2$—of 5–6 nm in size, and the size values observed for the $[1Co(OH)_2–1Pt(0)]_{10}$ sample, are significantly lower than those determined by the SEM method when analyzing the images in Fig. 1a. Apparently, in the case of SEM images, only agglomerates of smaller nanoparticles are visible in microphotographs, which cannot be directly observed by this method due to insufficiently high resolution. The smaller size of Pt(0) nanoparticles in the the sample obtained using the $[1Co(OH)_2–1Pt(0)]_{10}$ synthesis program can probably be explained by the smaller number of cycles at which they grow, and also by the possible blocking of crystallization centers of Pt(0) nanoparticles by cobalt hydroxide nanosheets formed on the surface at each cycle of treatment with reagents.

Conclusions about the crystal structure of multilayers can be drawn taking into account the interpretation of diffraction patterns given in Fig. 3. However, before analyzing these results, we note that the objects of this study were $[20Co(OH)_2]_1$, $[1Co(OH)_2–1Pt(0)]_{20}$, and $[5Co(OH)_2–5Pt(0)]_4$ multilayers, i.e. the multilayers obtained with a greater total number of SILD cycles and therefore having a greater thickness than those considered above. The choice of these synthesis conditions was made in view of the fact that it was not possible to reliably record diffraction patterns for the samples obtained with

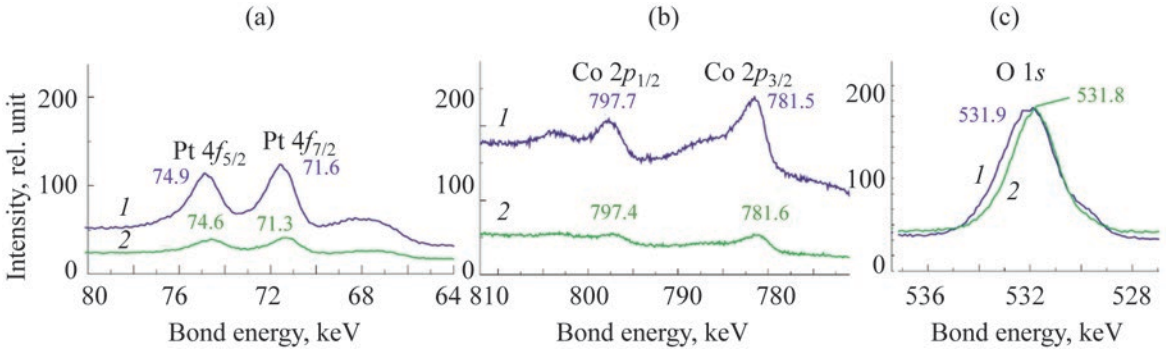

Fig. 4. X-ray photoelectron spectra of (a) Pt(0) 4*f* electrons, (b) Co 2*p* electrons, and (c) O 1*s* electrons of (*1*) $[5Co(OH)_2–5Pt(0)]_4$ and (*2*) $[1Co(OH)_2–1Pt(0)]_{10}$ multilayers synthesized by the SILD method on the nickel surface.

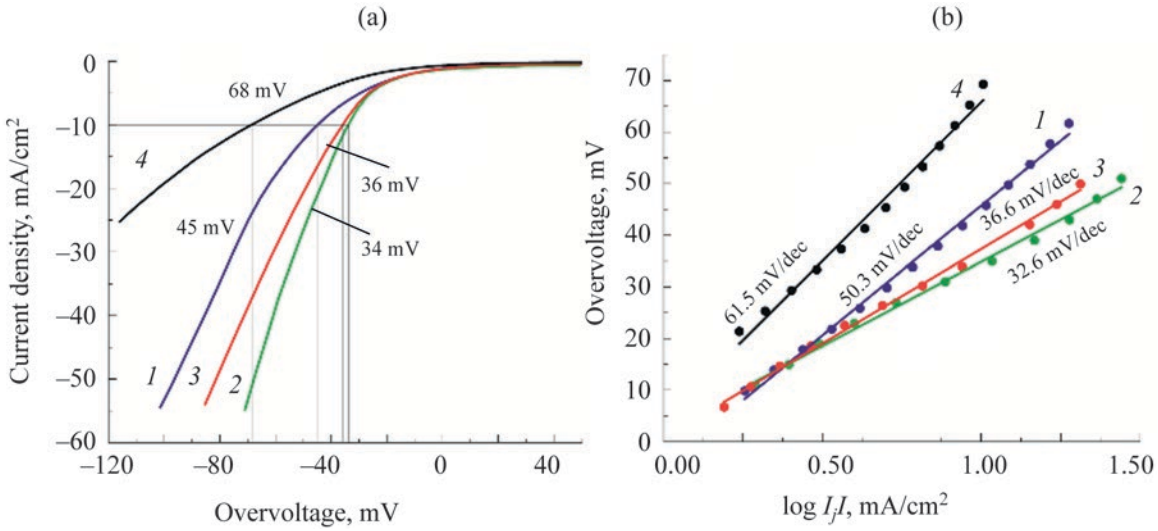

Fig. 5. (a) Polarization curves and (b) Tafel slopes in hydrogen evolution reaction for nickel foam electrodes with $[nCo(OH)_2–mPt(0)]_1$ multilayers synthesized by the SILD method. m = 10, (*1*) n = 0, (*2*) 5, (*3*) 10, and (*4*) 20.

a smaller number of cycles. On (2) and (4) diffraction patterns shown in Fig. 3, broad peaks are noticeable in the region of 20 deg, which, in our opinion, are due to diffraction from the (001) and (110) planes in $Co(OH)_2$ nanosheets with a hexagonal crystal structure [22]. It is noteworthy that X-ray diffraction pattern *3* of the sample synthesized using the $[1Co(OH)_2–1Pt(0)]_{20}$ algorithm does not show such peaks, and this is most likely due to the extremely small size of such nanosheets.

In the XPS spectra of the samples in Fig. 4, there are peaks at 781.6 and 781.5 eV characteristic of $2p_{3/2}$ electrons of Co atoms [23], and peaks at 71.6 and 71.3 eV, related to $4f_{7/2}$ electrons of Pt atoms [24]. Important information can also be obtained by analyzing the XPS spectra of 1*s* electrons of oxygen atoms (Fig. 4c). According to [25], the positions of the corresponding peaks at 531.9 and 531.8 eV indicate the formation of chemical bonds of oxygen atoms with cobalt and hydrogen atoms.

The study of the electrocatalytic properties of a number of synthesized samples in the HER during the electrolysis of water in an alkaline medium showed that the overpotential for $[0Co(OH)_2–10Pt(0)]_1$ at a current of 10 mA/cm^2 in HER was 45 mV, for $[5Co(OH)_2–10Pt(0)]_1$—34, for $[10Co(OH)_2–10Pt(0)]_1$—36, and for $[20Co(OH)_2–10Pt(0)]_1$—68 mV

(Fig. 5a). This series of samples is also characterized by Tafel slopes, which vary from 32.6 mV/dec to 61.5 mV/dec (Fig. 5b). These values indicate that the $[5Co(OH)_2–10Pt(0)]_1$ sample is the best, and apparently, it is for this sample that, on the one hand, the largest number of catalytically active centers is achieved on the surface, and, on the other hand, an interlayer of $Co(OH)_2$ nanosheets has a comparatively smaller thickness and does not make a significant contribution to the conductivity decrease.

In this work, in addition to the samples in Fig. 5, we studied the electrocatalytic properties of other samples (not shown in the figure), and it turned out that the best of them was $[5Co(OH)_2–5Pt(0)]_4$, which is characterized by an overpotential value of 31 mV and a Tafel slope value of 38.4 mV/dec.

Thus, it was shown for the first time by the example of the SILD synthesis of $[n(Co(OH)_2–mPt(0)]_k$ multilayers, that it is possible to obtain surface multilayers consisting of $Co(OH)_2$ nanosheets and Pt(0) nanoparticles by changing the sequence of the substrate treatment with $CoCl_2$, Na_2PtCl_6, and $NaBH_4$ solutions by the SILD method. The morphology of the multilayers can be controlled by changing, for example, the number and sequence of treatment cycles with reagents. It is important that such an approach to the synthesis opens up the possibility of controlled changes in a number of practically important properties of such multilayers, in particular, electrocatalytic properties relevant for the hydrogen production by the electrolysis of water in the alkaline region. Moreover, it is relatively easy to choose the mode of synthesis of products with optimal properties.

EXPERIMENTAL

Plates of nickel foam (NF) PPI 110 and nickel foil (Ni, 99.9%) with dimensions of about 8×15 mm were used as substrates for synthesis. Before synthesis, all substrates were, under ultrasonic treatment, washed with acetone and etched for 15 min in a 3 M HCl solution heated to 60°C. The NF substrates were used for electrochemical measurements, and foils were used to study the structural and chemical features of the synthesized layers using physical methods.

The reagents were aqueous solutions of $CoCl_2·6H_2O$ (Vekton), $H_2PtCl_6·6H_2O$ (Aurat), $NaBH_4$ (Sigma-Aldrich), and NaOH (Vekton). The pH value of the H_2PtCl_6 solution was 7.0; it was achieved by adding NaOH solution to the equilibrium solution of H_2PtCl_6. At this pH, the formation of Na_2PtCl_6 was observed and, therefore, it can be assumed that a solution of this particular salt was used as one of the reagents for the synthesis. The pH value of the $NaBH_4$ solution was equilibrium. All reagents were of analytical grade; reagent solutions were prepared using deionized water.

At the first stage of synthesis, when a $Co(OH)_2$ layer was obtained on the nickel surface, its plates were immersed in a 0.01 M $CoCl_2$ solution, then, after keeping it for 30 s, they were removed and washed with distilled water to remove excess reagent and reaction products. Then, at the second stage, they were immersed in a 1.0 M $NaBH_4$ solution, and after keeping in it for 30 s, they were also removed and washed again with distilled water. This sequence of treatments formed one SILD cycle, which was repeated many times. In the synthesis of Pt(0) nanoparticles, the sequence and times of treatments were similar, except that a Na_2PtCl_6 solution was used instead of a $Co(OH)_2$ solution. The syntheses were performed at room temperature and atmospheric pressure. After synthesis, the samples were dried in air at 60°C.

When applying multilayers, the number of SILD cycles during the synthesis of each of the components was set in accordance with the selected program.

Electron micrographs were obtained using a Zeiss Merlin scanning electron microscope and a Zeiss Libra 200 transmission electron microscope. The composition of the synthesized layers was characterized by XPS, the spectra were obtained using an ESCALAB 250Xi electron spectrometer with AlK_α radiation.

Electrochemical measurements were carried out on an Elins P-30I potentiostat by way of example of the hydrogen evolution during the electrolysis of water in an alkaline medium using a three-electrode cell with a graphite rod as an auxiliary electrode, and Hg/HgO (NaOH)—as a reference electrode. The working electrode was prepared by applying $[n(Co(OH)_2–mPt(0)]_k$ multilayers to the surface of the NF by the SILD method. The measurements were performed in 1 M KOH aqueous solution at room temperature and atmospheric pressure with a scanning speed of 5 mV/s, taking into account *iR* compensation. The Nernst equation was used to calculate the overvoltage.

ACKNOWLEDGMENTS

The studies were carried out using the equipment of the Resource Centers “Physical Methods of Surface Research,”

"Nanotechnologies," and "X-Ray Diffraction Research Methods" of St. Petersburg State University.

FUNDING

This work was supported by the Russian Science Foundation (grant no. 18-19-00370-P).

CONFLICT OF INTEREST

No conflict of interest was declared by the authors.

REFERENCES

1. Malygin, A.A., Drozd, V.E., Malkov, A.A., and Smirnov, V.M., *Chem. Vap. Dep*., 2015, vol. 21, p. 216. https://doi.org/10.1002/cvde.201502013
2. Bisengaliev, R.A., Novikov, B.V., Aleskovskiĭ, V.B., Drozd, V.E., Ageev, D.A., Gubaĭdullin, V.I., and Savchenko, A.P., *Phys. Solid State*, 1998, vol. 40, no. 5, p. 754. https://doi.org/10.1134/1.1130441
3. Doyle, S., Ryan, L., McCarthy, M.M., Modreanu, M., Schmidt, M., Laffir, F., Povey, I.M., and Pemble, M.E., *Mater. Adv*., 2022, vol. 3, p. 2896. https://doi.org/10.1039/D1MA00726B
4. Lee, L., Hwang, J., Jung, J.W., Kim, J., Lee, H.I., Heo, S., Yoon, M., Choi, S., Long, N.V., Park, J., Jeong, J. W., Kim, J., Kim, K.R., Kim, D.H., Im, S., l, Lee, B.H., and Cho, K., *Nat. Commun*., 2019, no. 10, p. 1998. https://doi.org/10.1038/s41467-019-09998-x
5. Lobinsky, A.A. and Tolstoy, V.P., *RSC Adv*., 2018, no. 8, p. 29607. https://doi.org/10.1039/C8RA00671G
6. Lobinsky, A.A. and Tolstoy, V.P., *J. Sol. St. Chem*., 2014, vol. 270, p. 156. https://doi.org/10.1016/j.jssc.2018.09.041
7. Popkov, V.I. and Tolstoy, V.P., *Surf. Coat. Techn*., 2021, vol. 409, p. 126914. https://doi.org/10.1016/j.surfcoat.2021.126914
8. Menshchikov, V.S., Belenov, S.V., Guterman, V.E., Novomlinskiy, I.N., Nevel'skaya, A.K., and Nikulin, A.Yu., *Russ. J. Electrochem*., 2018, vol. 54, no. 11, p. 937. https://doi.org/10.1134/S1023193518130293
9. Zhang, S.L., Lu, X.F., Wu, Z.-P., Luan, D., and Wen, X., *Angew. Chem. Int. Ed*., 2021, vol. 60, p. 19068. https://doi.org/10.1002/anie.202106547
10. Wu, H., Zuo, X., Wang, S.-P., Yin, J.-W., Zhang, Y.-N., and Chen, J., *Prog. Nat. Sci.: Mater*., 2019, vol. 29, p. 356. https://doi.org/10.1016/j.pnsc.2019.05.009
11. Xing, Z., Han, C., Wang, D., Li, Q., and Yang, X., *CS Catal*., 2017, vol. 7, p. 7131. https://doi.org/10.1021/acscatal.7b01994
12. Du, P., Wen, Y., Chiang, F.-K., Yao, A., Wang, J.-Q., Kang, J., Chen, L., Xie, G., Liu, X., and Qiu, H.-J., *ACS Appl. Mater. Interfaces*, 2019, vol. 11, p. 14745. https://doi.org/10.1021/acsami.8b22268
13. Skibina, L.M., Mauer, D.K., Volochaev, V.A., and Guterman, V.E., *Russ. J. Electrochem*., 2019, vol. 55, p. 438. https://doi.org/10.1134/S1023193519050136
14. Leont'ev, N., Guterman, V.E., Pakhomova, E.B., Guterman, A.V., and Mikheikin, A.S., *Nanotechn. Russ*., 2009, vol. 4, nos. 3–4, p. 170. https://doi.org/10.1134/S1995078009030045
15. Malik, B., Ananthara, S., Karthick, K., Pattanayak, D.K., and Kundu, S., *Catal. Sci. Technol*., 2017, vol. 7, p. 2486. https://doi.org/10.1039/C7CY00309A
16. Mauer, D., Belenov, S., Guterman, V., Nikolsky, A., Kozakov, A., Nikulin, A., Alexeenko, D., and Safronenko, O., *Catalysts*, 2021, vol. 11, p. 1539. https://doi.org/10.3390/catal11121539
17. Tolstoy, V.P., Lobinsky, A.A., and Kaneva, M.V., *J. Mol. Liq*., 2019, vol. 282, p. 32. https://doi.org/10.1016/j.molliq.2019.02.067
18. Kaneva, M.V., Gulina, L.B., and Tolstoy, V.P., *J. Alloys Compd*., 2022, vol. 901, p. 163640. https://doi.org/10.1016/j.jallcom.2022.163640
19. Bodhankar, P. M., Sarawade, P.B., Singh, G., Vinu, A., and Dhawale, D.S., *J. Mater. Chem. A*, 2021, vol. 9, p. 3180. https://doi.org/10.1039/D0TA10712C
20. Tang, S., Li, X., Courte, M., Peng, J., and Fichou, D., *Inorg. Chem. Front*., 2020, vol. 7, p. 2241. https://doi.org/10.1039/D0QI00318B
21. Bodhankar, P.M., Sarawade, P.B., Singh, G., Vinu, A., and Dhawale, D.S., *J. Mater. Chem. A*, 2021, vol. 9, no. 6, p. 3180. https://doi.org/10.1039/d0ta10712c
22. Liu, S., Tan, X., Zheng, X., and Liang, S., *Ionics*, 2020, vol. 26, p. 3531. https://doi.org/10.1007/s11581-020-03491-y
23. Cole, K.M., Kirk, D.W., and Thorpe, S.J., *Surf. Sci. Spectra*, 2020, vol. 27, p. 024013. https://doi.org/10.1116/6.0000318
24. Vovk, E.I., Kalinkin, A.V., Smirnov, M.Yu., Klembovskii, I.O., and Bukhtiyarov, V.I., *J. Phys. Chem. C*, 2017, vol. 121, p. 17297. https://doi.org/10.1021/acs.jpcc.7b04569
25. Biesinger, M.C, Payne, B.P., Grosvenor, A.P., Lau, L.W.M., Gerson, A.R., and Smart, R.St.C., *Appl. Surface Sci.*, 2011, vol. 257, p. 2717. https://doi.org/10.1016/j.apsusc.2010.07.086